AIP Journal of Applied Physics

Effect of surface structure on workfunction and Schottky-barrier height in SrRuO3/SrTiO3 (001) heterojunctions

V. Sampath Kumar and Manish K. Niranjan

Citation: Journal of Applied Physics **115**, 173705 (2014); doi: 10.1063/1.4872466
View online: http://dx.doi.org/10.1063/1.4872466
View Table of Contents: http://scitation.aip.org/content/aip/journal/jap/115/17?ver=pdfcov
Published by the AIP Publishing

Effect of surface structure on workfunction and Schottky-barrier height in $SrRuO_3/SrTiO_3$ (001) heterojunctions

V. Sampath Kumar and Manish K. Niranjan[a)]
Department of Physics, Indian Institute of Technology, Hyderabad, India

(Received 30 January 2014; accepted 13 April 2014; published online 6 May 2014)

We present an *ab-initio* theoretical study of work functions and surface energies of $SrRuO_3$ (001) surfaces and Schottky-barrier heights (SBHs) at various interfaces in $SrRuO_3/SrTiO_3$ (001) heterostructure within the framework of the density-functional theory. The $SrRuO_3$ workfunctions are found to exhibit strong dependence on surface terminations. The workfunction of two defect-free $SrRuO_3$ (001) surface terminations, viz., SrO and RuO_2, differ by as much as 2.37 eV. The *p*-type SBH at the $RuO_2/SrO/TiO_2$ interface is calculated to be 1.27 eV. The substitution of interfacial SrO layer by isoelectronic BaO layer induces small change in the *p*-SBH (~0.06 eV). However, the *p*-SBH is reduced significantly (~0.5 eV) as the RuO_2 layer is substituted by MnO_2 layer due to large change in the interfacial dipole. The *p*-SBH at different interfaces in $SrRuO_3/SrTiO_3$ structures are also estimated using semi-empirical metal-induced-gap-states (MIGS) model. The estimated values are found to be larger by ~2 eV than those obtained using *ab-initio* method, rendering the validity of MIGS model questionable in the prediction of SBH in all-oxide metal/dielectric heterojunctions. The modification of SBH by interfacial doping offers the possibility of contact resistance control in $SrRuO_3/SrTiO_3$ heterostructures and related devices.
 [http://dx.doi.org/10.1063/1.4872466]

I. INTRODUCTION

Complex oxide heterostructures have stimulated intense research activity in past few years.[1–10] The oxides are immensely promising for technological applications as they offer novel device concepts and functionalities. These materials are now widely used in devices such as sensors, actuators, accelerometers[11] and have opened new frontiers in oxide-based nanoelectronics and spintronics.[6,8,9,11,12] Complex oxides are also interesting from fundamental scientific point of view as they exhibit wide spectrum of properties which results from coupling between charge, spin and orbital degrees of freedom.[3,7,13–18] Some of these properties are ferroelectricity, magnetism, high-temperature superconductivity, colossal magnetoresistance, and multiferroicity. Furthermore, many emergent phenomena such as interfacial magnetism,[19,20] two-dimensional electron gas formation,[21,22] interfacial superconductivity,[23] etc., have been observed in heterostructures composed of oxide materials with different functionalities. The successful integration of oxide heterostructures in modern electronic devices requires an in-depth understanding of physical mechanisms which affect their critical electronic properties.[11] One of the fundamental parameters that influences the characteristics of metal/oxide heterostructure, in particular the electron transport and capacitance behavior, is the Schottky-barrier formed at the interface.[24,25] In general, the Schottky barrier height (SBH) exhibits strong dependence on atomic structure of the interface in the heterostructure and is of fundamental interest as an intrinsic property of the system.[26]

The $SrRuO_3/SrTiO_3$ (001) heterostructure is a prototypical system to study SBH at the oxide metal/dielectric interface.[27–29] Here the $SrRuO_3$ (SRO) and $SrTiO_3$ (STO) are the metallic and insulating oxides crystallizing in perovskite structure. Recently, reversible resistance switching has been demonstrated at the Schottky interface in $SrRuO_3/Nb:SrTiO_3$ structure,[29] which has potential applications in resistance switcing random access memories. The origin of resistance switcing is attributed to variation in SBH. Morover the SRO has attracted a lot of attention in recent years as an electrode material of choice to make contacts to ultrathin ferroelectric films.[30,31] It has been demonstrated that the thickness of perovskite ferroelectric films with SRO electrodes can be reduced down to approximately three unit cells (~1.2 nm) due to screening of depolarizing field.[30] Interesting phenomena such as a large magnetoelectric coupling at the interface of dielectric or ferroelectric material and SRO have also been recently proposed, based on theoretical studies.[16] SRO has good electrical conductivity, high thermal stability, good lattice match with STO and with other functional soxides which makes it easy to integrate in oxide heterostructures. On the other hand, STO is a good insulating oxide, widely used as substrate material for growth of other oxides and layered high T_c superconductors. The high dielectric permitivity of STO also makes it useful for applications in variety of integrated devices.

Although SRO films have been investigated extensively, not much is known about SRO/STO heterostructure. In particular, the dependence of SRO work function on crystal orientation and surface termination is not known. Further the SBH at SRO/STO junction and its dependence on the interface structure is not properly understood. The theoretical estimate of the SBH and its sensitivity to the interface atomic structure can be obtained from *ab-initio* calculations.[32] These calculations also provide fundamental understanding of interfacial atomic and electronic structure, on which SBH ultimately depends. In past few years, experimental

[a)]E-mail: manish@iith.ac.in. Tel.: (91)040-23016092. Fax: (91)040-23016032

realization of oxide heterostructures with high atomic precision has become a reality thanks to advances in thin-film deposition and experimental characterization. In this regard, the *ab-initio* calculations can be very helpful in the theoretical design of various novel oxide heterostructures.

In this work, we present a study of SBH and its dependence on the interface structure in SRO/STO heterojunctions from first-principles and using semiempirical Metal-Induced-Gap-States (MIGS) model. We also calculate the workfunctions and surface enegetics of free SRO surfaces with different terminations which, in turn, are used to obtain the semiempirical estimates of the SBH.

II. COMPUTATIONAL METHODOLOGY AND INTERFACE MODELS

The calculations are performed within the framework of density-functional theory.[33] The ionic potentials are simulated using projected augmented wave (PAW) method, as implemented in the VASP package.[34] The Perdew–Burke–Ernzerhof (PBE)[35] form of the generalized gradient approximation for exchange and correlation is employed along with a plane wave basis set with a kinetic energy cutoff of 500 eV. The supercell calculations are performed using the Monkhorst-Pack $12\times12\times1$ k-points mesh. The calculations are converged to 10^{-6} eV/cell and all supercell structures are relaxed until the largest force on each atom becomes less than 0.01 eV/A°. The overall accuracy of the Schottky-barrier estimates is expected to be of the order of 0.1 eV.

We first briefly review the electronic structure of SRO and STO. The calculated total density of states (DOS) and site projected density of states (PDOS) for SRO and STO with high symmetry cubic perovskite structure $(Pm\bar{3}m)$ are shown in Fig. 1. The metallic nature of SRO is apparent from non-zero density of states (Fig. 1(a)) at the Fermi level. The states below the Fermi energy in SRO are derived primarily from the hybridization of Ru-4*d* orbitals and O-2*p* orbitals. The calculated magnetic moment for SRO comes out to be 1.28 μ_B per Ru and is in good agreement with the reported experimental value which lies between 1.4 μ_B/Ru and 1.7 μ_B/Ru.[36] In Fig. 1(e), the band gap between valence and conduction band shows that STO is insulating. Further it is clear from Figs. 1(f)–1(h) that the main contribution to DOS below valence band maximum and above conduction band minimum in STO comes from the hybridization between Sr-4d and O-2p orbitals and Ti-3d and O-2p orbitals, respectively. These results are in good agreement with other previously reported theoretical studies.[37,38]

The oxide interfaces are simulated using supercell geometries with three-dimensional periodic boundary conditions. The supercells are composed of 4.5 unit cells of SRO on top of 6.5 unit cells of STO along [001] direction (see Fig. 2). To check the convergence of results, larger supercells consisting 8.5 units cells of SRO and 6.5 unit cells of STO are also used. Assuming STO is substrate, the in-plane lattice parameters of SRO/STO supercell are kept fixed to experimental value of lattice constant of bulk STO

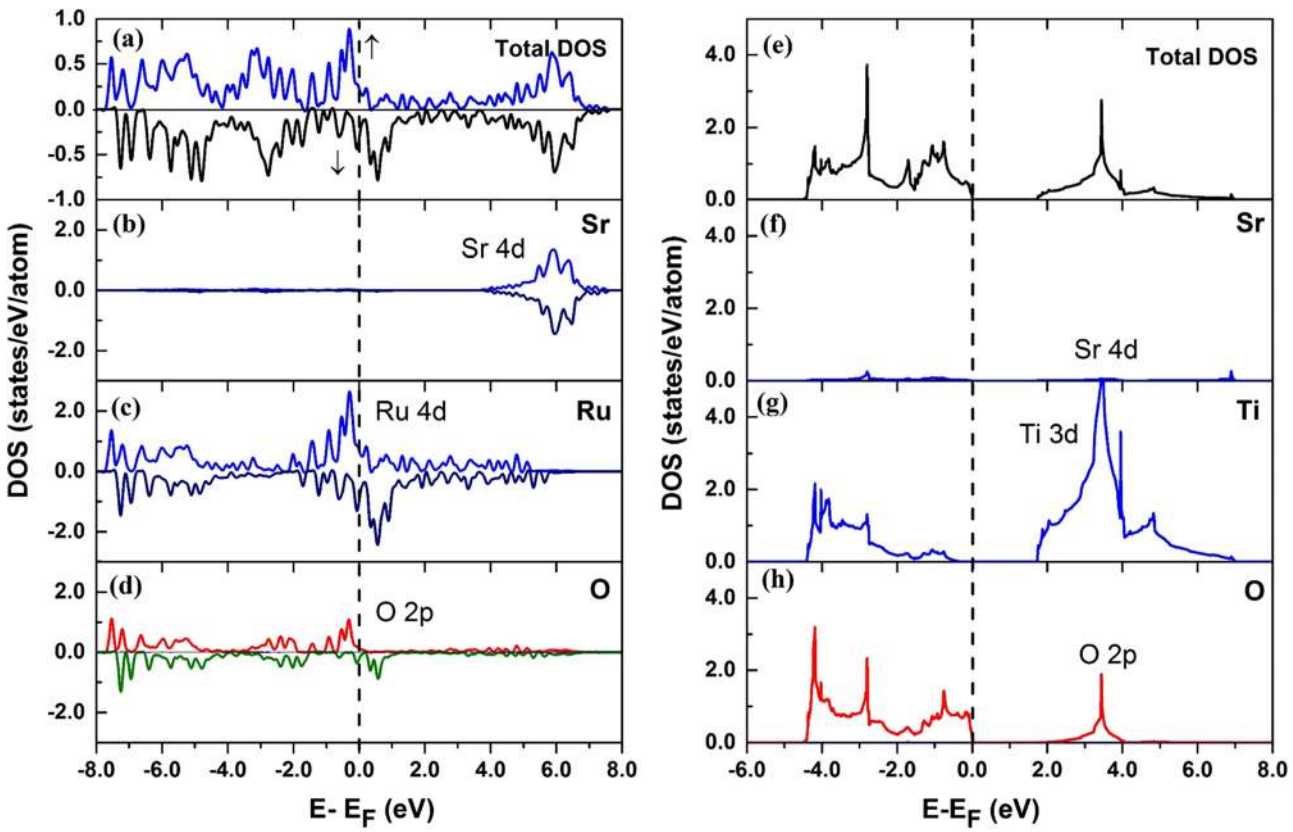

FIG. 1. (a) The total density of states of SRO (b) the PDOS of SRO projected onto Sr atom, (c) PDOS of SRO projected onto Ru atom, (d) PDOS of SRO projected onto O atom. (e) The total density of states of STO. (f) PDOS of STO projected onto Sr atom. (g) PDOS of STO projected onto Ti atom. (d) PDOS of STO projected onto O atom.

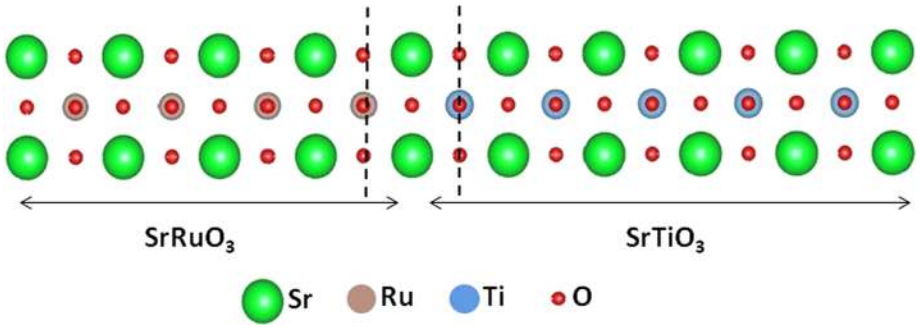

FIG. 2. Side view of the atomic structure of SRO/STO supercell with $RuO_2/SrO/TiO_2$ interface.

($\mathbf{a}_{STO} = 3.905$ Å). This results in 1.81% misfit strain in SrRuO3 film. The lattice constant in direction normal to the interface and atomic coordinates are optimized by minimizing energy of the supercell. The elongation in direction normal to the interface accommodates the compressive strain in SRO film. The ABO_3 perovskite structure has regular staking of AO and BO_2 layers. Since SrO sublattice is common to both SRO and STO, the SRO/STO (001) heterostructure has only one defect-free interface structure, i.e., $RuO_2/SrO/TiO_2$. In addition to this interface structure, we study supercell with interfaces such as $RuO_2/BaO/TiO_2$ and $SrO/MnO_2/SrO$ to study the sensitivity of SBH on interface structure. These interfaces are created by replacing one monolayer (ML) of SrO with BaO and one ML of RuO_2 with MnO_2 at the interface in $RuO_2/SrO/TiO_2$ and $SrO/RuO_2/SrO$ interface supercells. The BaO layer is chosen since it is isoelectronic to SrO layer, whereas the choice of MnO_2 is motivated by its strong magnetic properties as compared to RuO_2 layer.

III. SURFACE ENERGETICS AND WORK FUNCTIONS

A. Surface energies of $SrRuO_3$(001) and SrTiO3(001) surfaces

We calculate energies of SRO(001) surfaces with SrO and RuO_2 terminations and STO(001) surfaces with SrO and TiO_2 terminations in slab geometries which consist eight unit cells of SRO(STO) followed by six unit cells of vacuum (~24 A°). In the simplified picture, the SrO and RuO_2 (TiO_2) planes can be considered as independent units in the SRO/vacuum slab.[39] The formation energy ΔH_f needed to make bulk $SrRuO_3$ from SrO and RuO_2 per formula unit is defined as

$$-\Delta H_f = E_{SrRuO_3} - E_{SrO} - E_{RuO2}, \tag{1}$$

where E_{SrRuO3}, E_{SrO}, and E_{RuO2} are energies of bulk $SrRuO_3$, SrO, and RuO_2 per formula unit in cubic perovskite, cubic rock salt and rutile structures, respectively. A similar equation is valid in case of $SrTiO_3$. The calculated formation energies for SRO and STO are 0.22 eV and 1.2 eV, respectively. Assuming the system is in equilibrium with a reservoir of bulk $SrRuO_3$, the formation energy can be expressed as

$$\mu_{SrO} + \mu_{RuO2} = -\Delta H_f, \tag{2}$$

where μ_{SrO} and μ_{RuO2} are chemical potentials of SrO and RuO_2. The chemical potentials are measured with respect to their bulk phase value ($\mu_{Bulk} = 0$). Thus, $\mu_{SrO} = 0$ and $\mu_{RuO2} = 0$ corresponds to a system in contact with bulk SrO and RuO_2, respectively. The surface energy of the $SrRuO_3$ surface is estimated using the Gibbs free energy approach and is given by

$$F = \frac{1}{2A}[E_{slab} - N_{SrO}(E_{SrO} + \mu_{SrO}) - N_{RuO2}(E_{RuO2} + \mu_{RuO2})]. \tag{3}$$

In our calculations, the μ_{SrO} is chosen as an independent parameter and is restricted to the energy range bounded by its bulk value and $SrRuO_3$ formation energy.

$$-\Delta H_f \leq \mu_{SrO} \leq 0. \tag{4}$$

At $\mu_{SrO} = -\Delta H_f$, the system is in equilibrium with RuO_2 and $SrRuO_3$. The value of μ_{SrO} lower than the formation energy corresponds to precipitation of bulk RuO_2. Likewise the value higher than zero corresponds to precipitation of bulk SrO. In Fig. 3(a), the energies of RuO_2 and SrO terminated $SrRuO_3$(001) surfaces are shown. As evident the SrO terminated surface has lower energy than RuO_2 terminated surface by ~1000 erg/cm^2 in the energy range shown in Eq. (4). The lower and upper limit of μ_{SrO} corresponds to RuO_2 and SrO rich conditions, respectively. The energies of TiO_2 and SrO terminated $SrTiO_3$(001) surfaces are shown in Fig. 3(b). As can be seen, under SrO-rich condition the energy of SrO-terminated $SrTiO_3$(001) surface is lower than TiO_2-terminated surface by ~1000 erg/cm^2 and remains lower in energy for μ_{SrO} ranging from 0 to −0.98 eV. However, under TiO_2-rich conditions, the TiO_2-terminated surface has lower energy than SrO-terminated surface by ~200 erg/cm^2. The energy crossover takes place relatively under TiO_2 rich conditions at $\mu_{SrO} \sim -1.0$ eV.

B. Work functions of SrO and RuO_2 terminated $SrRuO_3$ (001) surfaces

The work function of SRO (001) surfaces with SrO and RuO_2 terminations are calculated in a slab geometry which consists eight unit cell of SRO followed by six unit cells of vacuum (~24 Å). We also calculate workfunctions of SRO (001) surfaces with BaO and MnO_2 terminations. These surface terminations are created by replacing SrO and RuO_2 surfaces by single ML of BaO and MnO_2. The work function is calculated using the identity $\varphi_m = E_{vac} - E_{Fermi}$. Here, E_{vac} and E_{Fermi} are the vacuum energy and Fermi level, respectively. Fig. 4 show the vacuum energy E_{vac} as the total electrostatic potential in the vacuum region separating periodic images of the slab. The work function generally depends on the orientation of metal surface where a dipole

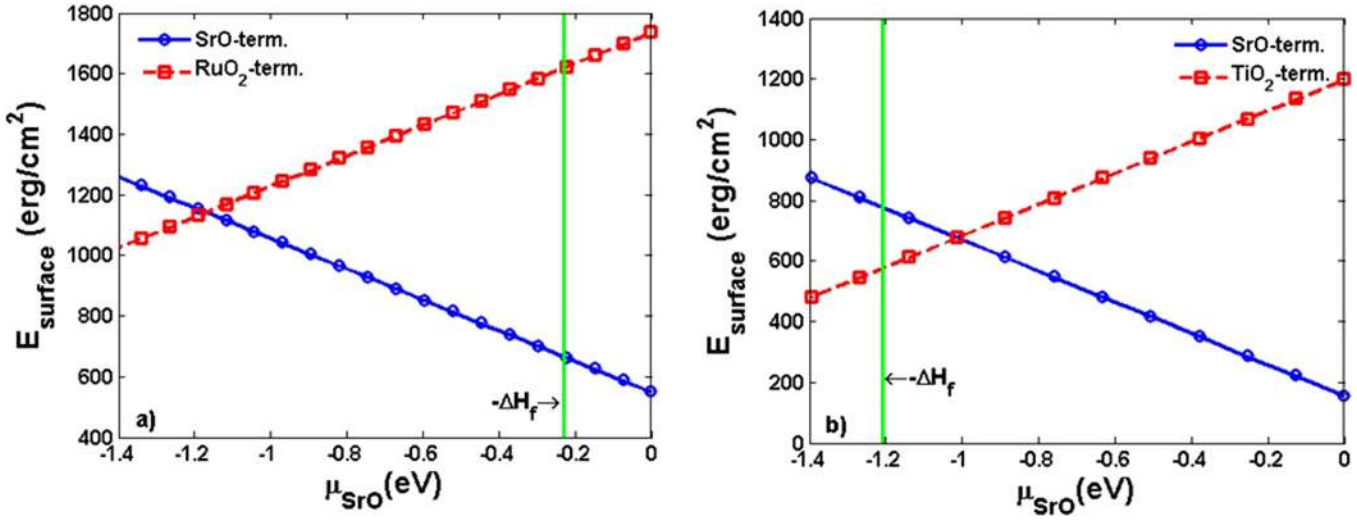

FIG. 3. Energies of (a) SrO- and RuO_2-terminated $SrRuO_3$(001) surfaces (b) SrO- and TiO_2-terminated $SrTiO_3$(001) surfaces. The vertical line indicates the formation energy. The chemical potential is restricted to energy range bounded by the bulk value (0 eV) and the formation energy.

barrier is formed due to redistribution of surface charge density. For elemental metals, the workfunction is known to vary from ~0.1 eV to ~1 eV.[24] It has been suggested that the variation in work function is primarily due to two competing effects on the surface dipole layer. The first is the charge spilling out at the surface, resulting in the formation of negative dipole layer which increases the workfunction. The second effect is the tendency to smoothen out the surface, resulting in the formation of a positive dipole layer, which tends to lower the work function. Table I shows the calculated workfunctions of SRO (001) surfaces with various terminations. It can be seen that the workfunction of RuO_2 terminated surface is larger by 2.37 eV than that of with SrO termination. The calculated value of RuO_2 terminated surface is 5.03 eV and is in good agreement with the experimental value of 5.2 eV.[40] However, no experimental reports exist on surface dependent SRO workfunctions to best of our knowledge rendering the direct comparison between theoretical and experimental values a bit ambiguous. Table I also shows the workfunction values obtained from the non-spin polarized calculations. As expected the effect of spin polarization is significant on MnO_2 terminated SRO workfunction. The large difference in the workfunction can be understood from the variation in the surface dipole layer induced by different charge and number density of SrO and RuO_2 surfaces. As can be seen in Table I, the workfunction is reduced to 1.72 eV as the surface SrO layer is replaced by BaO layer, whereas it is increased to 6.04 eV as surface RuO_2 layer is replaced by MnO_2 layer.

It is interesting to examine the validity of a recently proposed generic relation between the work function and the Young's modulus in case of SRO. The Young modulus (E) and the work function (φ) of a polycrystalline elemental metal appear to satisfy following relation:[41]

$$E = \alpha \frac{18 \times 16^6 \pi^{10} \hbar^6 \varepsilon_0{}^9}{e^{16} m^3} \varphi^6 \propto \alpha \varphi^6, \tag{5}$$

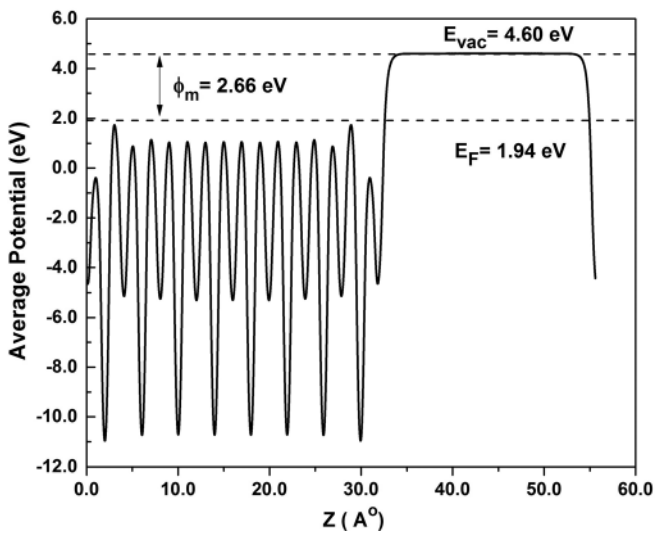

FIG. 4. The planar macroscopic averaged coulomb potential and work function of SrO-terminated SRO(001) surface. Z is the direction normal to the (001) surface.

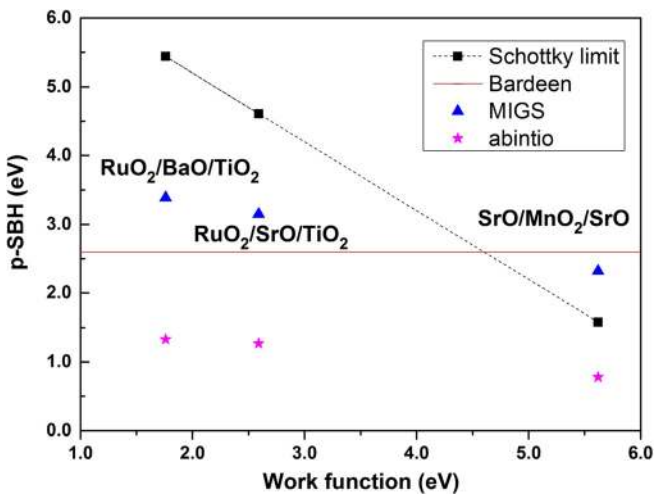

FIG. 5. The p-SBH at different interfaces in SRO/STO heterostructure as a function of SRO work function calculated using semiempirical models and ab-intio method.

TABLE I. The calculated work functions of $SrRuO_3$ (001) surfaces for different terminations. The values from non-spin and spin polarized calculations are shown.

	Workfunction (eV)			
Surface term. →	SrO	RuO_2	BaO	MnO_2
Non-spin pol.	2.66	5.03	1.74	5.64
Spin-pol.	2.52	5.0	1.72	6.04

where $\hbar$ is the Planck's constant, ε_0 is the vacuum permittivity, α is the Madelung constant, e is the elementary charge, and m is the mass of electron. The relation in Eq. (5) can be written as

$$E_{metal} = a_{metal} \times \varphi^6_{metal}. \tag{6}$$

The calculated value of a_{metal} from Eq. (6) is 0.02233. The Young modulus and workfunction are expressed in GPa and eV, respectively. In our calculations the Young's modulus (E) of SRO comes out to be 196.4 GPa, which is 22% higher than the reported experimental value of 161 GPa measured at the room temperature.[42] Since theoretical DFT value of E corresponds to that obtained at 0 K, a $\sim$10% reduction in its room temperature value is expected.[43] Taking workfunction for RuO_2 terminated (001) surface as 5.03 eV (see Table I), the calculated value of a_{SRO} comes out to be 0.012. The value of a_{SRO} comes out to be 0.008 with experimental values of E and φ, viz., 161 GPa and 5.2 eV, respectively. It is clear that the value of a_{SRO} is larger than a_{metal} by a factor of $\sim$2. The discrepancy is expected because of relatively more complex nature of electronic structure and atomic bonding in SRO.

IV. SCHOTTKY BARRIER HEIGHT AT THE $SrRuO_3/SrTiO_3$ (001) INTERFACES

We calculate the SBH in SRO/STO(001) supercells with different type of interface terminations using semiempirical models as well as *ab-intio* method. We also investigate the effect on SBH by replacing one ML of SrO and RuO_2 at the interface by BaO and MnO_2 layers, respectively. Over the past few decades, extensive studies have been performed on SBH formation at metal-semiconductor (M-S) interfaces and as consequence several phenomenological models have been proposed to explain the mechanisms of its formation. However, to date there exist no satisfactory generic model which can predict the SBH at any given M-S interface. Further, strong evidences suggest that interface atomic structure and bonding play a crucial role in the determination of SBH. The p-type SBH (ϕ_p) at the M-S interface is given as the difference between the valance band edge and the Fermi level (E_F) in the dielectric band gap.[24] The SBH generally lies between no-pinning limit and the strong-pinning limit and is determined by both metal work function and interface states.[25] The no-pinning limit of p-SBH is basically the ideal limit whereby the SBH varies linearly with metal workfunction. In this limit, the p-SBH is given as the difference between the sum of dielectric band gap (E_g) and electron affinity (χ), and metal workfunction (φ_m). The workfunction (φ_m) of SRO(001) free surfaces with different surface terminations are shown in Table I. We use experimental value of energy gap (3.2 eV) and electron affinity (3.9 eV) of STO since DFT values of these parameters are generally underestimated. In strong-pinning limit, the p-SBH does not show any dependence on metal work function due to Fermi level pinning at the charge neutrality level (ϕ_{CNL}) of the dielectric surface states. Basically, the ϕ_{CNL} is the position of the Fermi level which renders the semiconductor surface neutral.[24] In the strong pinning limit, the p-SBH is given as the difference between the charge neutrality level (ϕ_{CNL}) and valance band top of the semiconductor. The charge neutrality level ϕ_{CNL} of STO has been calculated as the branch point of the complex band structure of the semiconductor and found to be 2.6 eV above the valance band.[44] The p-SBH in this limit is same for all interface structures. However, a more improved estimate of p-SBH can be obtained using MIGS model.[45–47] This model is a linear interpolation between strong-pinning and no-pinning limits and given as

$$\phi_p = \varphi_{CNL} - S(\varphi_m - \chi - E_g + \varphi_{CNL}). \tag{7}$$

Here, ϕ_{CNL} is the charge neutrality level measured from the valence band top, E_g is the band gap of the insulator (STO), and φ_m is the work function of the metal (SRO). The pinning parameter S describes the screening by interfacial states and is characteristic of the insulator.[46]

$$S = \frac{1}{1 + 0.1(\varepsilon_\infty - 1)^2}, \tag{8}$$

where ε_∞ is the high frequency limit of the dielectric constant. The value of ε_∞ for STO is 6.1,[44] giving S equal to 0.28. The $S = 0$ and $S = 1$ correspond to strong-pinning and no-pinning limits of p-SBH, respectively. The calculated p-type barrier heights obtained from aforementioned models in SRO/STO heterostructure with different interface terminations are shown in Table II. In no-pinning limit, ϕ_p varies linearly with the SRO workfunction, whereas it is 2.6 eV in

TABLE II. The p-SBH at different interfaces in SRO/STO heterostructure calculated using semiempirical models and *ab-intio* method. The MA and LDOS indicate the values obtained using macroscopic averaging method and local density-of-states method, respectively. The non-spin and spin indicate the values obtained from non-spin polarized and spin polarized calculations.

	p-SBH ϕ_p (eV)		
Interface →	$RuO_2/SrO/TiO_2$	$RuO_2/BaO/TiO_2$	$SrO/MnO_2/SrO$
Semiempirical models			
Schottky–Mott	4.54	5.46	1.56
Bardeen Model	2.60		
MIGS	3.14	3.39	2.31
Ab-intio			
MA (No-spin)	1.40	1.42	1.03
(spin)	1.27	1.33	0.78
LDOS (No-spin)	1.33	1.35	0.96
(spin)	1.15	1.30	0.70

strong pinning limit for all interfaces. The MIGS estimate of p-SBH comes out to be 3.14, 3.39, and 2.31 eV for $RuO_2/SrO/TiO_2$, $RuO_2/BaO/TiO_2$, and $SrO/MnO_2/SrO$ interfaces, respectively. The semiemiprical methods are useful in providing the quick estimates and an insight into the physical mechanisms of SBH formation. However, there are number of limitations with such models, for instance, they are unable to describe dependence of SBH on the interface structure and resulting charge transfer. Recently, Tung[25,26] has proposed a bond polarization theory of Schottky-barrier whereby the Schottky dipole at the M/S interface is identified with the polarization of the interfacial chemical bonds. In this model the SBH is given as

$$\phi_p = \gamma_B(I_S - \varphi_m) + (1 - \gamma_B)\varphi_{CNL}, \tag{9}$$

where I_S and γ_B are the ionization potential of the semiconductor and the strength of the interface dipole. The γ_B is given as

$$\gamma_B = 1 - \frac{e^2 N_B d_{MS}}{\varepsilon_{\text{int}}(E_g + \kappa)}. \tag{10}$$

Here, d_{MS} is the distance between metal and semiconductor atoms at the interface, N_{B} is the density of the chemical bonds at the M/S interface, ε_{int} is the dielectric screening at the interface and κ is the sum of all hopping interactions between interfacial atoms. The dependence of SBH on the interface atomic structure and bonding can be described using *ab-initio* calculations with significant accuracy. We perform *ab-initio* calculations of the p-SBH in SRO/STO heterostructure with different type of supercells as explained in Sec. II (see Fig. 2). The p-SBH at SRO/STO interface is calculated from the formula

$$\phi_p = E_F - (\bar{V}_{\text{STO}} + E_{VBM}), \tag{11}$$

where the E_{F}, E_{VBM}, and $\bar{V}$STO are the Fermi energy, valance band edge position of STO, and the macroscopic average (MA) potential of STO in SRO/STO supercell, respectively. Fig. 6 shows the planar average of the electrostatic potential across the supercell. The macroscopic average $\bar{V}$STO is calculated in the region away from the interface. In this region, the STO electronic states have the bulk like character. The valence band maximum in bulk STO with respect to macroscopic average potential comes out to be 2.52 eV. The Fermi energy and macroscopic average of STO away from the interface in the supercell are 4.23 eV and 0.31 eV, respectively. Using Eq. (11), we calculate p-SBH of 1.40 eV for $RuO_2/SrO/TiO_2$ interface. This is in close agreement with previously reported p-SBH value for this interface.[48] We also infer p-SBH from the local density-of-states (LDOS) in SRO/STO supercell. The DOS projected on p-orbitals of O atom located on each layer of the supercell with $RuO_2/SrO/TiO_2$ interface is shown in Fig. 7. The p-SBH is calculated as the difference between Fermi level and the valance band top of STO in Fig. 7. Table II shows the p-SBH at different interfaces obtained using MA and LDOS methods. We also calculate the effect of spin-polarization on the p-SBH

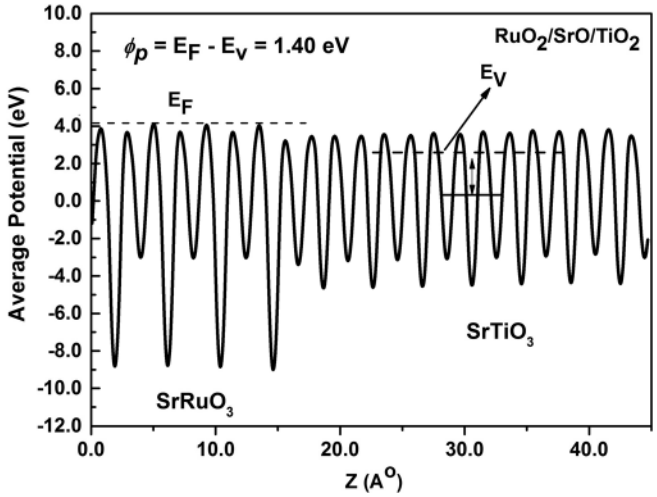

FIG. 6. The average coulomb potential (in eV) in $RuO_2/SrO/TiO_2$ terminated supercell along Z (slab axis).

at interfaces. The calculated p-SBH (using MA and LDOS methods with spin-polarization) at $RuO_2/SrO/TiO_2$, $RuO_2/BaO/TiO_2$, and $SrO/MnO_2/SrO$ are 1.27, 1.33, and 0.78 eV, respectively. As evident, the p-SBH is changed by a small value (0.06 eV) as the interfacial SrO layer is replaced by isoelectronic BaO layer. However it is significantly lowered ($\sim$0.5 eV) as RuO_2 layer is substituted with MnO_2 at the interface. As clear from the Table II, the barrier height is changed by $\sim$0.1 to 0.3 eV when the spin-polarization is taken

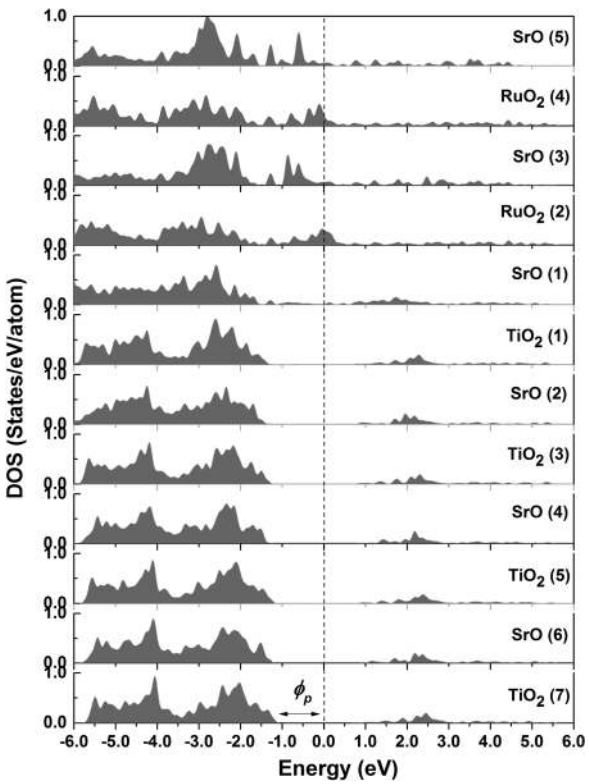

FIG. 7. Local spin-up density of states (LDOS) of the oxygen atoms in the $RuO_2/SrO/TiO_2$ interface in the SRO/STO heterostructure. The number indicates the layer number from the interface.

into account in the calculations. Further, as expected, the effect of spin-polarization on *p*-SBH is more pronounced in case of SrO/MnO_2/SrO interface. The *p*-SBH at different interfaces in SRO/STO heterostructure as a function of SRO work function calculated using ab-initio method and semiempirical models is shown in Fig. 5. To check the accuracy of our calculations with respect to supercell size, we have calculated the SBH using larger supercell (30 Layers). The obtained *p*-SBH values are within ~0.1 eV with those calculated with smaller supercell (see Table II). It is clear from Table II, that the *p*-SBH values calculated from the semi-empirical MIGS model differ significantly from its value calculated from *ab-initio* method. Though MIGS has been found to provide reasonable estimate of SBH at metal/semiconductor interfaces, its validity in case of metal/dielectric oxide interfaces is questionable.

V. CONCLUSIONS

We have studied the work functions and surface energetics of SrO- and RuO_2-terminated SRO (001) surfaces with different surface terminations and the *p*-SBH at different interfaces in SRO/STO (001) heterostructure using *ab-initio* density-functional theory. The energy of SrO-terminated surface of SRO remains lower by ~1000 erg/cm^2 than that of RuO_2-terminated surface for SrO as well as RuO_2 rich conditions reflected in permissible values of independent chemical potential parameter. However, in case of STO, the SrO- and TiO_2-terminated surfaces are energetically favorable for SrO and TiO_2 rich conditions, respectively.

The workfunction of SRO(001) surface with RuO_2 termination is found to be larger by 2.37 eV than that with SrO termination thereby showing strong dependence on surface termination. The calculated *p*-SBH at the RuO_2/SrO/TiO_2 interface in the SRO/STO system is 1.27 eV. The substitution of interfacial SrO layer by BaO layer results in insignificant change (~0.06 eV) in *p*-SBH. However the *p*-SBH is reduced by ~0.5 eV as the interfacial RuO_2 layer is substituted by MnO_2 layer. The *p*-SBH obtained using semi-empirical MIGS model is larger by ~2 eV than that obtained using *ab-initio* method. These results are very interesting from scientific and application point of view and we hope that our results will stimulate further experimental and theoretical studies in this field.

ACKNOWLEDGMENTS

The author thanks to High Performance Computing (HPC) facility at IIT Hyderabad (India) for providing computational resources for this work.

[1]J. Mannhart and D. G. Schlom, Science **327**(5973), 1607–1611 (2010).
[2]A. P. Ramirez, Science **315**, 1377–1378 (2007).
[3]*Multifunctional Oxide Heterostructure*, edited by E. Y. Tsymbal, E. R. A. Dagotto, C.-B. Eom, and R. Ramesh (Oxford University Press, UK, 2012).
[4]H. W. Jang, D. A. Felker, C. W. Bark, Y. Wang, M. K. Niranjan, C. T. Nelson, Y. Zhang, D. Su, C. M. Folkman, S. H. Baek, S. Lee, K. Janicka, Y. Zhu, X. Q. Pan, D. D. Fong, E. Y. Tsymbal, M. S. Rzchowski, and C. B. Eom, Science **331**(6019), 886–889 (2011).
[5]M. Bibes, J. E. Villegas, and A. Bethelemy, Adv. Phys. **60**, 5 (2011).
[6]C. Cen, S. Thiel, J. Mannhart, and J. Levy, Science **323**(5917), 1026 (2009).
[7]*Thin Films and Heterostructures for Oxide Electronics*, edited by S. Ogale (Springer, New York, 2005), pp. 251–278.
[8]B. Forg, C. Richter, and J. Manhart, Appl. Phys. Lett. **100**, 053506 (2012).
[9]P. Irvin, M. Huang, F. J. Wong, T. D. Sanders, Y. Suzuki, and J. Levy, Appl. Phys. Lett. **102**, 103113 (2013).
[10]P. Zubko, S. Gariglio, M. Gabay, P. Ghosez, and J. M. Triscone, Ann. Rev. Condensed Matter Phys. **2**, 141–165 (2011).
[11]M. Dawber, K. M. Rabe, and J. F. Scott, Rev. Mod. Phys. **77**, 1083 (2005).
[12]E. Y. Tsymbal and H. Kohlstedt, Science **313**, 181 (2006).
[13]E. Dagotto, Science **318**, 1076–1077 (2007).
[14]P. Yu, Y. H. Chu, and R. Ramesh, Philos. Trans. R. Soc. A **370**, 4856–4871 (2012).
[15]A. Tsukazaki, A. Ohtomo, T. Kita, Y. Ohno, H. Ohno, and M. Kawasaki, Science **315**, 1388–1391 (2007).
[16]M. K. Niranjan, J. D. Burton, J. P. Velev, S. S. Jaswal, and E. Y. Tsymbal, Appl. Phys. Lett. **95**, 052501 (2009).
[17]J. P. Velev, C. G. Duan, J. D. Burton, A. Smogunov, M. K. Niranjan, E. Tosatti, S. S. Jaswal, and E. Y. Tsymbal, Nano Lett. **9**, 427 (2009).
[18]M. K. Niranjan, J. P. Velev, C.-G. Duan, S. S. Jaswal, and E. Y. Tsymbal, Phys. Rev. B **78**, 104405 (2008).
[19]V. Garcia, M. Bibes, L. Bocher, S. Valencia, F. Kronast, A. Crassous, X. Moya, S. Enouz-Vedrenne, A. Gloter, D. Imhoff, C. Deranlot, N. D. Mathur, S. Fusil, K. Bouzehouane, and A. Barthélémy, Science **327**, 1106 (2010).
[20]M. K. Niranjan, C.-G. Duan, S. S. Jaswal, and E. Y. Tsymbal, Appl. Phys. Lett. **96**, 222504 (2010).
[21]A. Ohtomo and H. Y. Hwang, Nature **427**(6973), 423 (2004).
[22]M. K. Niranjan, Y. Wang, S. S. Jaswal, and E. Y. Tsymbal, Phys. Rev. Lett. **103**, 016804 (2009).
[23]N. Reyren, S. Thiel, A. D. Caviglia, L. F. Kourkoutis, G. Hammerl, C. Richter, C. W. Schneider, T. Kopp, A.-S. Rüetschi, D. Jaccard, M. Gabay, D. A. Muller, J.-M. Triscone, and J. Mannhart, Science **317**, 1196 (2007).
[24]S. M. Sze, *Physics of Semiconductor Devices*, 2nd ed. (Wiley, New York, 1981).
[25]R. T. Tung, Mater. Sci. Eng. **35**, 1 (2001).
[26]R. T. Tung, Appl. Phys. Rev. **1**, 011304 (2014).
[27]Y. Hikita, Y. Kozuka, T. Susaki, H. Takagi, and H. Y. Hwang, Appl. Phys. Lett. **90**, 143507 (2007).
[28]S. Roy, A. M. Kamerbeek, K. G. Rana, S. Parui, and T. Banerjee, Appl. Phys. Lett. **102**, 192909 (2013).
[29]T. Fujii, M. Kawasaki, A. Sawa, H. Akoh, Y. Kawazoe, and Y. Tokura, Appl. Phys. Lett. **86**, 012107 (2005).
[30]D. D. Fong, G. B. Stephenson, S. K. Streiffer, J. A. Eastman, O. Auciello, P. H. Fuoss, and C. Thompson, Science **304**, 1650 (2004).
[31]J. Junquera and P. Ghosez, Nature **422**, 506 (2003).
[32]M. Peressi, N. Binggell, and A. Baldereschi, J. Phys. D: Appl. Phys. **31**, 1273 (1998).
[33]W. Kohn and L. J. Sham, Phys. Rev. **140**, A1133 (1965).
[34]G. Kresse and J. Furthmuller, Phys. Rev. B **54**, 11169 (1996).
[35]J. P. Perdew, K. Burke, and M. Ernzerhoff, Phys. Rev. Lett. **77**, 3865 (1996).
[36]P. B. Allen *et al.*, Phys. Rev. B **53**, 4393 (1996).
[37]C. E. Ekuma, M. Jarrell, J. Moreno, and D. Bagayoko, AIP Adv. **2**, 012189 (2012).
[38]E. Heifets, R. I. Eglitis, E. A. Kotomin, J. Maier, and G. Borstel, Surf. Sci. **513**, 211–220 (2002).
[39]J. Padilla and D. Vanderbilt, Phys. Rev. B **56**, 1625 (1997).
[40]X. Fang and T. Kobayashi, Appl. Phys. A: Mater. Sci. Process. A **69**, S587 (1999).
[41]G. Hua and D. Y. Li, Appl. Phys. Lett. **99**, 041907 (2011).
[42]S. Yamanaka, T. Maekawa, H. Muta, T. Matsuda, S. Kobayashi, and K. Kurosaki, J. Solid State Chem. **177**, 3484 (2004).
[43]T. Chi Duong, N. Singh, and R. Arróyave, Comput. Mater. Sci. **79**, 296 (2013).
[44]J. Robertson, J. Vac. Sci. Technol. B **18**, 1785 (2000).
[45]V. Heine, Phys. Rev. **138**, A1689 (1965).
[46]W. Monch, Phys. Rev. Lett. **58**, 1260 (1987).
[47]M. K. Niranjan, L. Kleinman, and A. A. Demkov, Phys. Rev. B **77**, 155316 (2008).
[48]J. M. Albina, M. Mrovec, B. Meyer, and C. Elsaesser, Phys. Rev. B **76**, 165103 (2007).